UNIVERSIDADE FEDERAL DE PELOTAS
Pró-Reitoria de Pesquisa, Pós-Graduação e Inovação
Centro de Ciências Químicas, Farmacêuticas e de Alimentos
Programa de Pós-Graduação em Química

EDITAL Nº 62/2020

SELEÇÃO DE ALUNO REGULAR - 2020/02

Programa recomendado pela CAPES, nível Mestrado, em 12 de julho de 2006.
Programa recomendado pela CAPES, nível Doutorado, em 1º de março de 2011.

Ao longo do artigo selecionado, discutem-se vários aspectos de desenvolvimento da Química. Nele, estão presentes questões que nos permitem analisar a Química desde sua área básica, como no caso das análises sobre a formação de ligação química, seu comprimento e estabilidades termodinâmica e cinética, até questões relacionadas ao desenvolvimento de técnicas e modelos mais recentes, como nos casos da análise por meio de nanotubos de carbono e o emprego de cálculos quânticos por via computacional.

Com base nessas características do artigo, elabore um documento, seguindo formatação típica de um artigo científico, que articule em um texto coerente:

i) Um panorama geral do texto;

ii) Uma discussão a respeito de ligações químicas, articulada com as questões destacadas no artigo;

iii) Relações entre o texto e o cenário recente da pesquisa em Química e suas subáreas, além de articulações com outros textos do campo da Química e áreas afins.

Uma boa prova!

Science Advances
AAAS

advances.sciencemag.org/cgi/content/full/6/3/eaay5849/DC1

Supplementary Materials for

Imaging an unsupported metal–metal bond in dirhenium molecules at the atomic scale

Kecheng Cao, Stephen T. Skowron, Johannes Biskupek, Craig T. Stoppiello, Christopher Leist, Elena Besley, Andrei N. Khlobystov*, Ute Kaiser*

*Corresponding author. Email: ute.kaiser@uni-ulm.de (U.K.); andrei.khlobystov@nottingham.ac.uk (A.N.K.)

Published 17 January 2020, *Sci. Adv.* **6**, eaay5849 (2020)
DOI: 10.1126/sciadv.aay5849

The PDF file includes:

Other Supplementary Material for this manuscript includes the following:

(available at advances.sciencemag.org/cgi/content/full/6/3/eaay5849/DC1)

Section S1. Re_2 electronic structure and choice of functional

The presence of strong interactions between the Re 6s-orbitals has the effect of raising the energy of the associated antibonding σ orbital to the region of the *δ*-orbitals *(12)*. This regime of "strong s-orbital overlap" gives rise to an electronic ground state containing a singly occupied antibonding σ orbital, which provides the open s-shell configuration that is generally required for favourable chemical bond formation in transition metal diatoms. (For the atomic ground states of the Group 7 elements, the nd orbitals are typically unable to interact and form bonds due to strong repulsion between the (n+1)s shells - excitation from these $(n+1)s^2\ nd^5$ states to the $(n+1)s^1\ nd^6$ states are required for bond formation to occur *(28)*.) Hence, rather than the ground state of the rhenium dimer being a closed shell singlet species ($d\sigma_g^{\ 2}\ d\pi_u^{\ 4}\ s\sigma_g^{\ 2}\ d\delta_g^{\ 4}\ s\sigma_u^{\ 2}$), it is an open shell triplet species ($d\sigma_g^{\ 2}\ d\pi_u^{\ 4}\ s\sigma_g^{\ 2}\ d\delta_g^{\ 4}\ s\sigma_u\ d\delta_u$).

The choice of exchange-correlation functional is especially important when modelling rhenium dimers and related species with density functional theory (DFT), as the multiplicity of the rhenium dimer ground electronic state is very sensitive to the choice of functional. The minimum energy of the triplet ground state lies especially close to the singlet state, within the accuracy of previously performed CASSCF/CASPT2 calculations *(28)* which required the inclusion of spin-orbit coupling to obtain results that agreed qualitatively with experimental studies. While local functionals quantitatively outperform hybrid functionals for modelling bonding between transition metals in general, *(29)* hybrid functionals fail to describe the electronic structure of the rhenium dimer even qualitatively (in many cases predicting a false quintet ground state) *(30,31)*. For a recent example see reference *(32)*, which used B3LYP/LANL2DZ to investigate Re_n (n = 2-16); use of the B3LYP functional resulted in the geometric analysis being performed on an incorrect ground state for the Re dimer.

Two local GGA functionals (PBE *(33)* and BLYP *(34,35)*) and one local meta-GGA functional (M06-L *(36)*) have been used to model the electronic structure of a single Re_2 dimer in the gas phase, chosen for their general accuracy in modelling structural and vibrational properties of transition metal complexes, as measured against experimental data and benchmark test suites *(29, 36)*. Each exchange-correlation functional was paired with four effective core potentials (ECPs) and associated valence-electron basis sets: LANL2DZ *(37)*, SRSC *(38)*, def2-SVP and def-TZVP *(39)*, all of which replace the [Kr]+4d+4f core orbitals. The energies of the lowest singlet, triplet, and quintet configuration of the Re dimer for each level of theory were compared to ensure that the correct triplet ground state was reproduced in each case. The ground state of the isolated rhenium atom is the high-spin sextet configuration, which was accurately reproduced for each of the three functionals. All calculations were performed using unrestricted DFT.

The M06-L functional greatly underestimates the bonding strength of the dimer, while also showing a very high sensitivity to the choice of ECP. Of the two GGA functional, BLYP most closely reproduces the experimentally measured bond lengths and frequencies, and SRSC is the best performing ECP. BLYP/SRSC correspondingly exhibits the best match to experiment, and was chosen as the combination of functional and ECP for subsequent calculations.

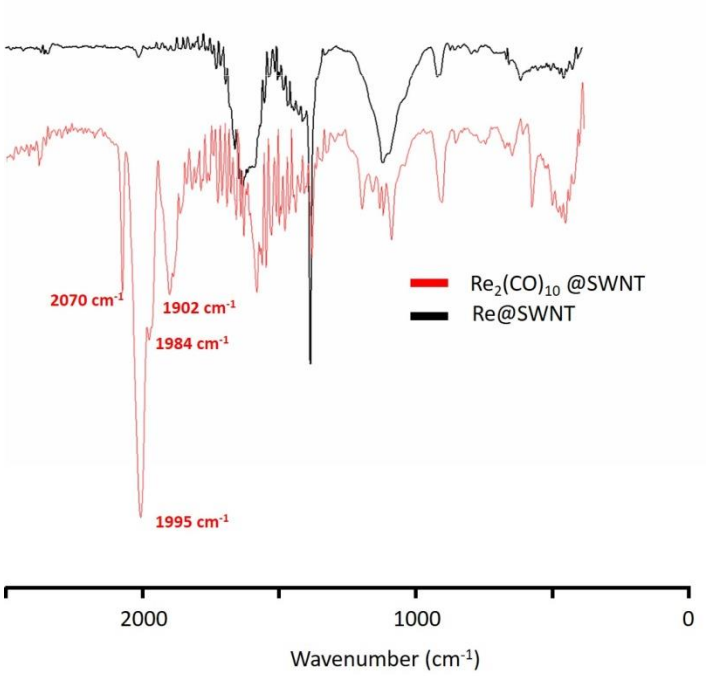

Fig. S1. Infrared spectra of Re_2 precursor before and after removal of CO ligands. FTIR of $Re_2(CO)_{10}$@SWNT (red) and Re@SWNT formed by thermal decomposition of $Re_2(CO)_{10}$@SWNT (black). The spectra show the characteristic bands of carbonyl group (1902 cm^{-1}, 1984 cm^{-1}, 1995 cm^{-1}, 2070 cm^{-1} as indicated) in $Re_2(CO)_{10}$@SWNT that disappeared after heat treatment indicating that the CO ligands have been removed from the nanotube.

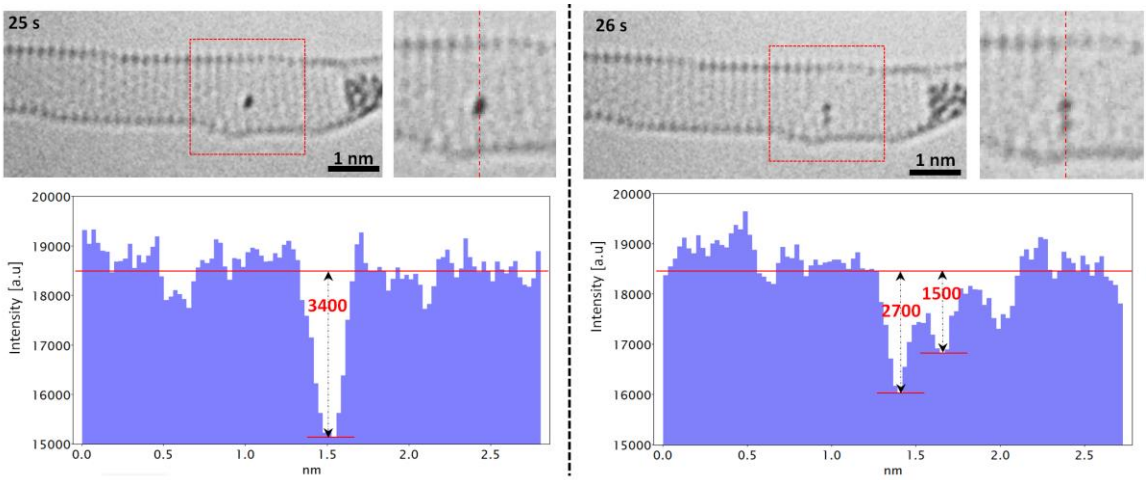

Fig. S2. Analysis of a typical migration process repeatedly observed in our TEM experiment. The Re_2 stands on the inner wall of SWNT at 25 s which shows one dark spot with intensity of 3400 in the AC-HRTEM image by analyzing profile of the dash line in the enlarged area. Both atoms of Re_2 can be observed in the following frame with exposure time of 1 second as shown in the AC-HRTEM image at 26 s. The different intensities of 2700 and 1500 demonstrate that the initial configuration existed for 0.29 seconds of the frame time, followed by 0.71 seconds in the second configuration, considering that the intensity of the spot is proportional to the time the atom spends in each position.

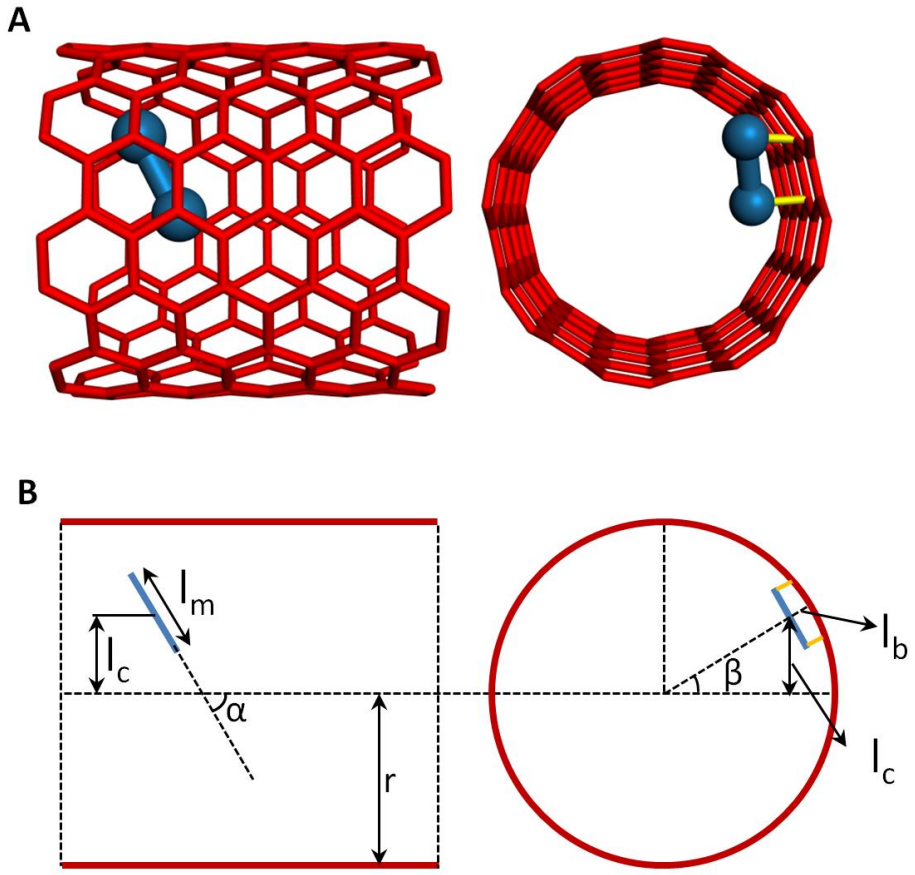

Fig. S3. Schematic diagram explaining the method for calculating the real bond length between two Re atoms in Re_2 by correcting the measured projected bond length. (A) Front and side views of molded structure of a Re_2 lying on the inner wall of SWNT. (B) Parameters in the cross and side profile for calculating the real bond length. l_m is the measured projected bond length of Re_2, r is the radius of the SWNT, l_c is the distance between the center of the Re_2 and the axis of SWNT in projection, α is the angle between the Re_2 and the axis of SWNT in projection, l_b is the distance between Re_2 and the inner wall of SWNT caused by Re-C bonding and is approximatively 0.20 nm. For the situation that Re_2 is on the outer wall of SWNT, l_b is - 0.20 nm for calculation. When the SWNT is perfect and without any deformation, the real bond length between two Re atoms in Re_2, l is

$$\boldsymbol{l = l_m + \left(1 + \frac{{l_c}^2 \times \sin \alpha^2}{(r - l_b)^2 - {l_c}^2}\right)^{\frac{1}{2}}} \qquad \text{Equation S1}$$

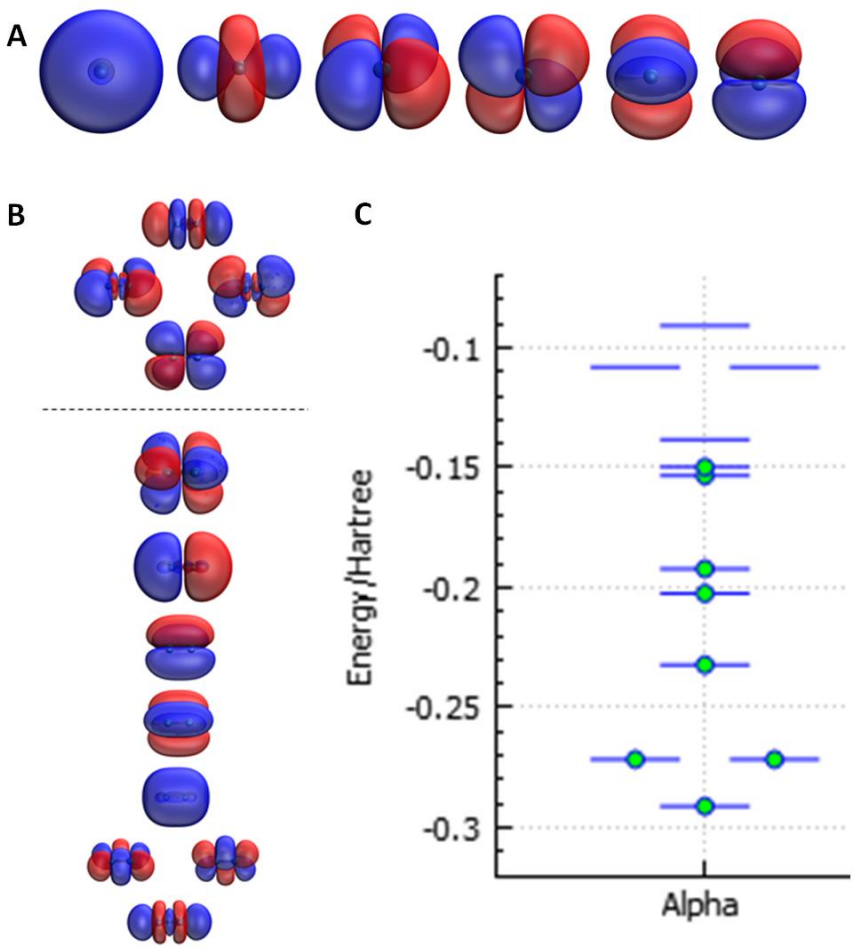

Fig. S4. Shapes and energies of Re_2 orbitals. (A) Atomic Re valence orbitals: 6s, 5 dz^2, dxz, dyz, dxy, dx^2-y^2 successively. (B) Occupied and low lying unoccupied orbitals of Re_2: $d\sigma_g^{\ 2}$ $d\pi_u^{\ 4}$ $s\sigma_g^{\ 2}$ $d\delta_g^{\ 4}$ $s\sigma_u$ $d\delta_u$ (the dotted line indicates the HOMO-LUMO gap), and relative energies in (C).

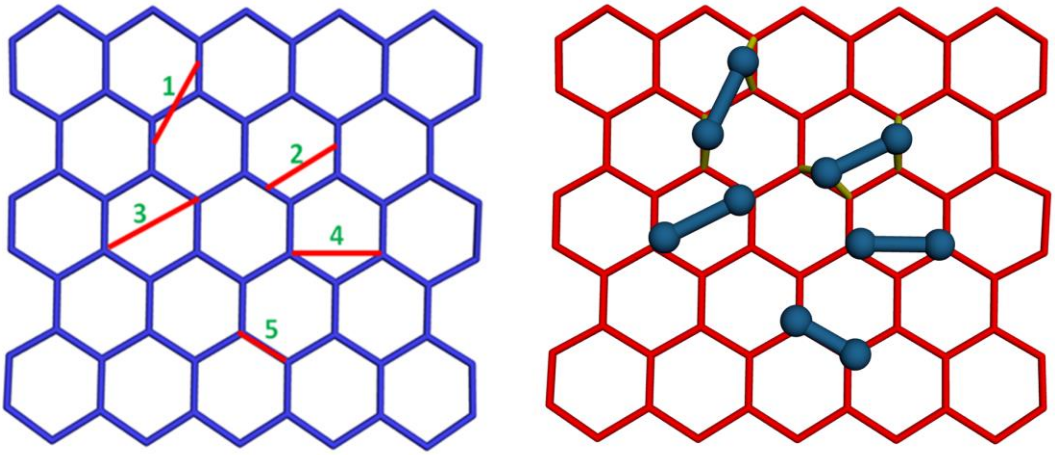

Fig. S5. Possible configurations of Re_2 lying on the graphitic structure. The configurations that Re_2 lying on the graphitic structure of SWNT from inside or outside have various possibilities. 5 of the possible configurations are presented. The configuration 1 and 2 show the Re_2 interacts with four carbon atoms in two different ways. The configuration 3, 4 and 5 show the Re_2 interacts with two carbon atoms in three different ways. These configurations were used as initial states in the DFT geometry optimizations (both inside and outside the tube) in addition to three standing states centered over a hexagon, a carbon-carbon bond, and a carbon atom. Several non-bonded initial configurations in which Re_2 was placed in the center of the SWNT (inside) or far from the SWNT wall (outside) were also used.

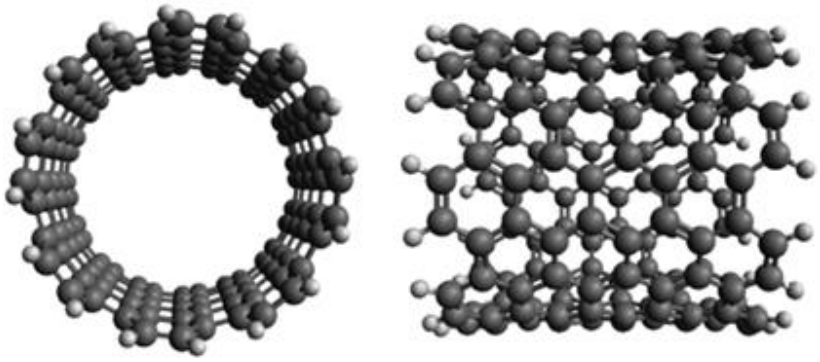

Fig. S6. The model SWNT system used in the DFT calculations discussed in the text. The SWNT has a chirality of (8, 8) and is terminated with hydrogen atoms.

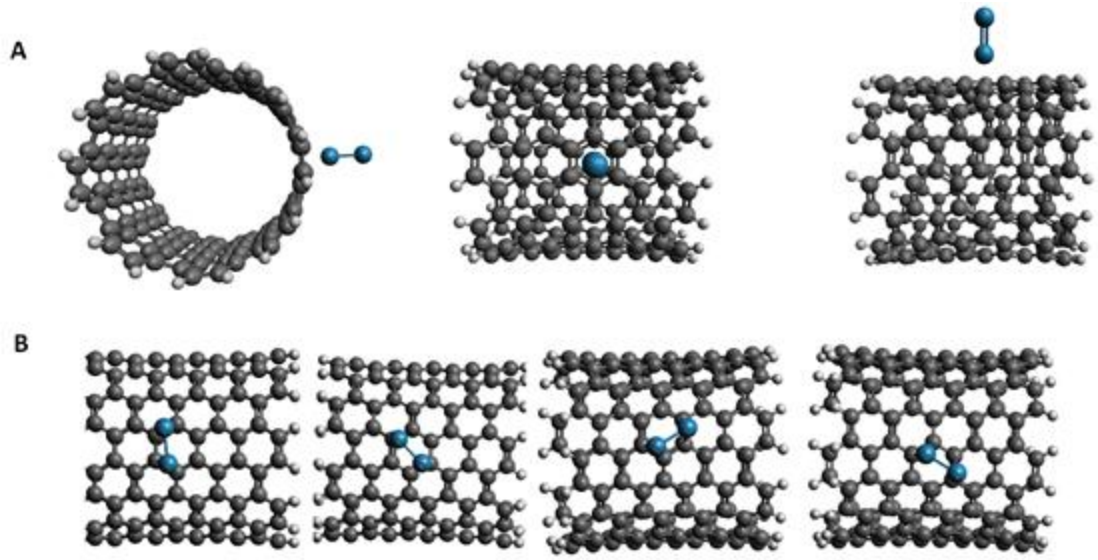

Fig. S7. Configurations of Re_2 outside SWNT with respect to the nanotube lattice. (A) Three views of the lowest energy configuration with Re_2 bonded to the outside of the SWNT. (B) Several additional stable bonding configurations, representing very small variations on a hybrid of the configurations labelled 2, 3 and 4 in fig. S5.

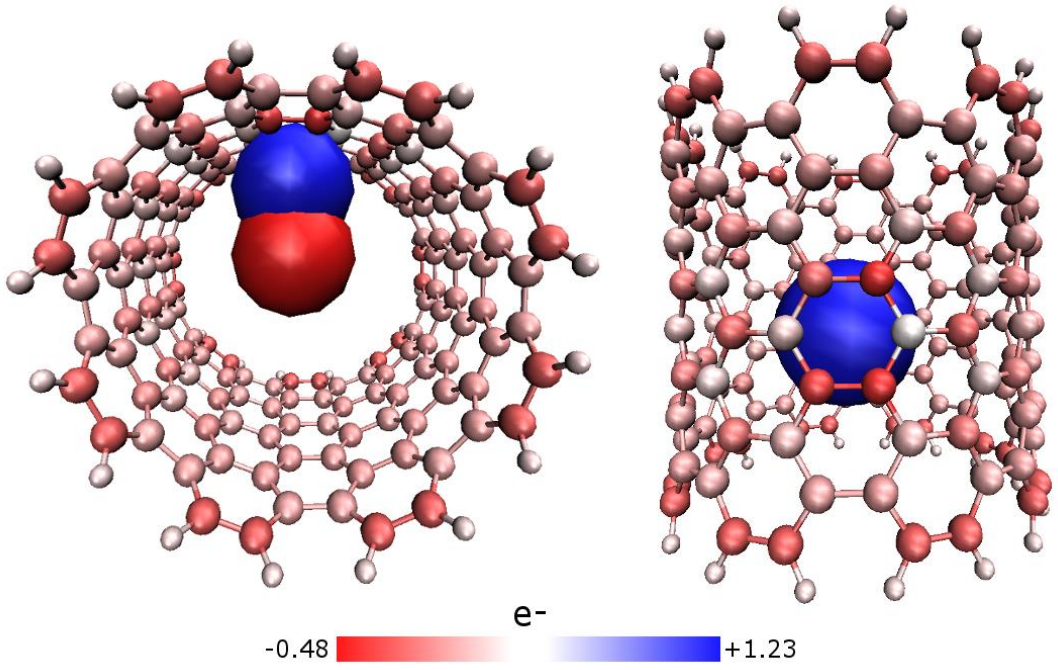

Fig. S8. The Mulliken charge distribution of the bonded standing state found in the DFT calculations. The net charge transfer from dirhenium to the SWNT is approximately 0.75 electrons.

Captions for Movies S1 to S2

Movie S1. Dynamics of two Re_2 molecules confined in SWNT stimulated and imaged by electron beam in Titan TEM at 80 kV. 227 frames with 1 second exposure time during 553 seconds are acquired.

Movie S2. Dynamics of one Re_2 molecule stimulated and imaged by electron beam in SALVE TEM at 80 kV. 382 frames with 0.5 second exposure time during 393 seconds are acquired.

MATERIALS SCIENCE

Imaging an unsupported metal–metal bond in dirhenium molecules at the atomic scale

Kecheng Cao[1], Stephen T. Skowron[2], Johannes Biskupek[1], Craig T. Stoppiello[2], Christopher Leist[1], Elena Besley[2], Andrei N. Khlobystov[2]*, Ute Kaiser[1]*

Metallic bonds remain one of the most important and least understood of the chemical bonds. In this study, we generated Re_2 molecules in which the Re–Re core is unsupported by ligands. Real-time imaging of the atomic-scale dynamics of Re_2 adsorbed on a graphitic lattice allows direct measurement of Re–Re bond lengths for individual molecules that changes in discrete steps correlating with bond order from one to four. Direct imaging of the Re–Re bond breaking process reveals a new bonding state with the bond order less than one and a high-amplitude vibrational stretch, preceding the bond dissociation. The methodology, based on aberration-corrected transmission electron microscopy imaging, is shown to be a powerful analytical tool for the investigation of dynamics of metallic bonding at the atomic level.

INTRODUCTION

Bonding between metal atoms is of fundamental importance to many areas of science and technology, including catalysis and magnetism (*1*), and since the discovery of the Re–Re quadruple bond in $[Re_2X_8]^{2-}$ in 1964 (*2*, *3*), the global effort in understanding the nature of the metal–metal (M–M) bond has been growing strongly (*1*). The key challenge is to establish the bond order of M–M, which can vary from one to five and determines fundamental physical and chemical properties (*1*). Spectroscopy methods such as nuclear magnetic resonance, infrared spectroscopy, ultraviolet-visible spectroscopy, and x-ray diffraction are typically used (*4*–*6*). The latter is particularly important, as it allows measurement of the M–M bond length, which is inversely proportional to the bond order. However, unlike bonds between nonmetallic elements, M–M bonds are very sensitive to ligands around the metals (*7*, *8*), creating the uncertainty whether the bond length and bond order reflect on the fundamental chemistry of the metals atoms or result from the effects of ligands, packing of molecules in the crystal or other external factors not related to the intrinsic M–M bonding. Encouraged by theoretical calculations predicting stable unsupported M–M bonds (*9*, *10*), the existence of homonuclear intermetallic bonds has been experimentally demonstrated in the noble gas matrices under cryogenic conditions (*11*, *12*), and more recently, the excited-state heteronuclear alkali metal diatomic molecule has been successfully obtained by combining two atoms with optical tweezers (*13*).

In this work, we create dirhenium molecules with unsupported Re–Re bonds using single-walled carbon nanotubes (SWNTs) as a nano–test tube while simultaneously imaging their structure and dynamics on the level of the single atom in real time using state-of-the-art chromatic and spherical aberration–corrected (C_C/C_S-corrected) SALVE (Sub Angstrom Low-Voltage Electron Microscopy) transmission electron microscopy (TEM) (*14*, *15*). Moving freely at room temperature along the SWNT, the Re_2 molecules have been shown to switch bond order between one, two, and four, and we could follow the process of dissociation and reformation of intermetallic bonds in individual Re_2 molecules.

RESULTS

Dirhenium molecules are generated from $Re_2(CO)_{10}$ compound inserted into SWNTs, followed by thermal or e^--beam–induced elimination of CO ligands (Fig. 1A). The dissociation of $Re_2(CO)_{10}$ molecules and the removal of CO ligands is confirmed by Fourier transform infrared spectroscopy (FTIR) measurements (fig. S1). If several precursor molecules $Re_2(CO)_{10}$ are agglomerated in the nanotube, they form a metal nanocluster with several Re atoms under these conditions (*16*, *17*); in the case of a single isolated molecule, $Re_2(CO)_{10}$ ligand elimination yields a well-defined Re_2 molecule as observed by aberration-corrected high-resolution TEM (AC-HRTEM) (three typical images of Re_2 are shown in Fig. 1A). Two individual dirhenium molecules can be observed in the same SWNT in the top AC-HRTEM image of Fig. 1A. Monitoring an individual Re_2 by time-series 80-kV AC-HRTEM imaging (Fig. 1B) shows that the two Re atoms are bonded to each other within the dirhenium molecule, as Re_2 moves as a whole in the cavity of SWNT, which differs notably from the dynamics of individual heavy atoms in graphitic structures that move by hopping from one vacancy defect in the carbon lattice to another under e-beam irradiation (*18*–*21*). The Re–Re bond ensures that the movement of both atoms is correlated, and the dirhenium molecule takes positions in the SWNT, consistent with small number of possible orientations: (i) chemisorbed standing (20 s), (ii) chemisorbed lying (0 s), and (iii) successive chemisorbed standing and lying configurations during the exposure time (26 s) (Fig. 1B). The same Re_2 molecule is able to change its position and orientation over the duration of the experiment. This process is stimulated by the e^--beam serving as both a source of energy and the imaging probe, as the kinetic energy of the incident electrons is transferred to the Re atoms (directly ~1.0 eV and via carbon atom ~14.7 eV). As the positions of the rhenium atoms are monitored continually during the exposure time of each frame (1 s), the motion of Re_2 switching from one orientation to another can be captured within a single frame and analyzed (see Fig. 2). For example, it is possible to discern that the change in the bonding orientation that takes place during the 26th second corresponds to a change from

[1]Central Facility for Materials Science Electron Microscopy, Ulm University, Albert-Einstein-Allee 11, Ulm 89081, Germany. [2]School of Chemistry, University of Nottingham, University Park, Nottingham NG7 2RD, UK.
*Corresponding author. Email: ute.kaiser@uni-ulm.de (U.K.); andrei.khlobystov@nottingham.ac.uk (A.N.K.)

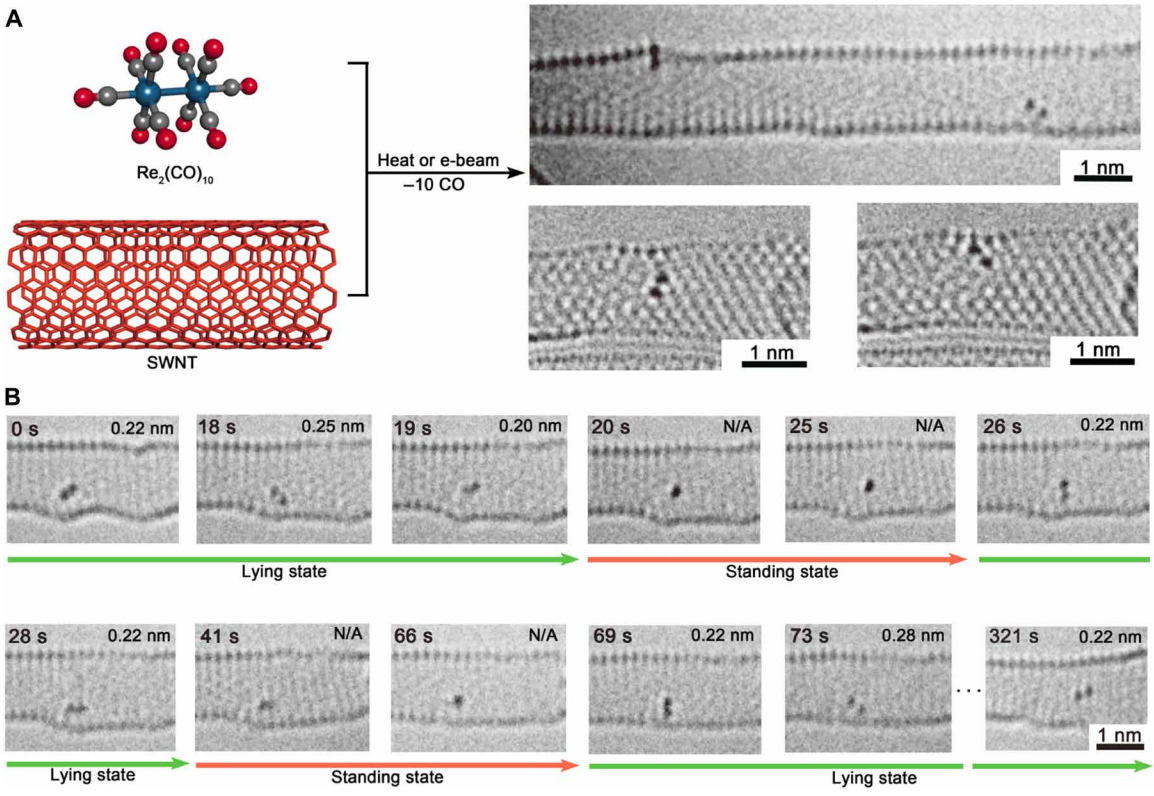

Fig. 1. Diatomic molecule Re_2 trapped in carbon nano–test tube. (**A**) Schematic illustration of the preparation of dirhenium molecule confined in SWNT by eliminating CO groups from $Re_2(CO)_{10}$ precursor. Three dirhenium molecules in two SWNTs can be observed in the AC-HRTEM images [two dirhenium molecules imaged at 80 kV with *C*s-corrected (top image) and one dirhenium molecule *C*c/*C*s-corrected (bottom two images) TEM, unprocessed data]. (**B**) Time-series AC-HRTEM images (80 kV) from movie S1 acquired by Titan C_S-corrected TEM showing the characteristic states of the dirhenium molecule changing under e^--beam irradiation. This dirhenium molecule is the right one in the SWNT of the top AC-HRTEM image in (A) named "Titan Re_2 A." The corrected Re–Re bond length of each frame is presented; error is ±0.015 nm. N/A is the standing state with unknown bond length.

the initial standing orientation lasting 0.29 s into the lying orientation lasting 0.71 s in the 1.0 s frame (fig. S2).

DISCUSSION

There is a well-known strong inverse correlation between the M–M bond length and bond order (*3*). The Re–Re single σ bond length in $Re_2(CO)_{10}$ is 0.304 nm for the free molecule and 0.302 nm in the crystal (*22*). However, in our experiments, after the CO ligands have been removed, the Re–Re bond measures 0.220 nm (± 0.015 nm) at the initial state (0 s; Fig. 1B), indicating that the bond order is close to four, as it agrees well with the length of a quadruple Re–Re bond in $[Re_2X_8]^{2-}$ of 0.224 nm (*2*). Our density functional theory (DFT) calculations for Re_2 match well with the experimentally observed distances, predicting Re–Re bond lengths of 0.21 nm for a free (nonbonded) Re_2 and approximately 0.22 nm for the dirhenium molecule bound to the SWNT wall by the stable standing orientation. Because the SWNTs are cylindrical surfaces, all the bond lengths quoted in this work are corrected from the directly measured projected distance using the method described in fig. S3. Statistical analysis of Re–Re bond lengths in 226 frames from 0 to 553 s (Fig. 2C) shows three major values of the length of 0.22, 0.25, and 0.30 nm, occurring with 44, 24, and 11% probability (Fig. 2E). The nonrandom, discrete values assumed by the Re–Re bond are likely to be correlated with the quadruple bond, double bond, and single bond, respectively, which were previously reported from bulk measurements on various complexes containing a Re_2 core (*3*, *22*). In additional 18% of the cases, the bond length cannot be measured as marked "N/A," as the "standing" state is aligned with the direction of the electron beam. Being limited by the spatial resolution of only spherical AC-TEM, the atomic structure of the SWNT and hence the precise position of the Re atoms with respect to the carbon lattice remain unresolved.

With the help of the C_C/C_S-corrected SALVE TEM, the e^--beam–stimulated dynamics of dirhenium molecule are recorded with a much higher spatial resolution, as shown in movie S2. A Re_2 molecule can be observed standing at defective sites on the top SWNT of two parallel SWNTs at the initial state (0 s; Fig. 2A shows the first stage of movie S2 from 0 to 87 s). A van der Waals (vdW) gap of 0.3 nm is formed by the two parallel SWNTs with different chirality. In the first 50 s, Re_2 shows similar behavior to the Re_2 in Fig. 1B, switching between multiple different orientations at the defective site. An intact SWNT is impermeable to almost all atoms and ions except H^+ (*23*). However, a vacancy defect on the SWNT could provide a channel for atoms to penetrate. At 50 s, one Re atom of the dirhenium molecule goes across the upper wall of the host SWNT from the defective site. In the following 20 s, the whole dirhenium molecule climbs out and starts drifting along the outer surface of the host SWNT, driven by stronger bonding of the metal with defect from outside, as was predicted by dynamic simulations

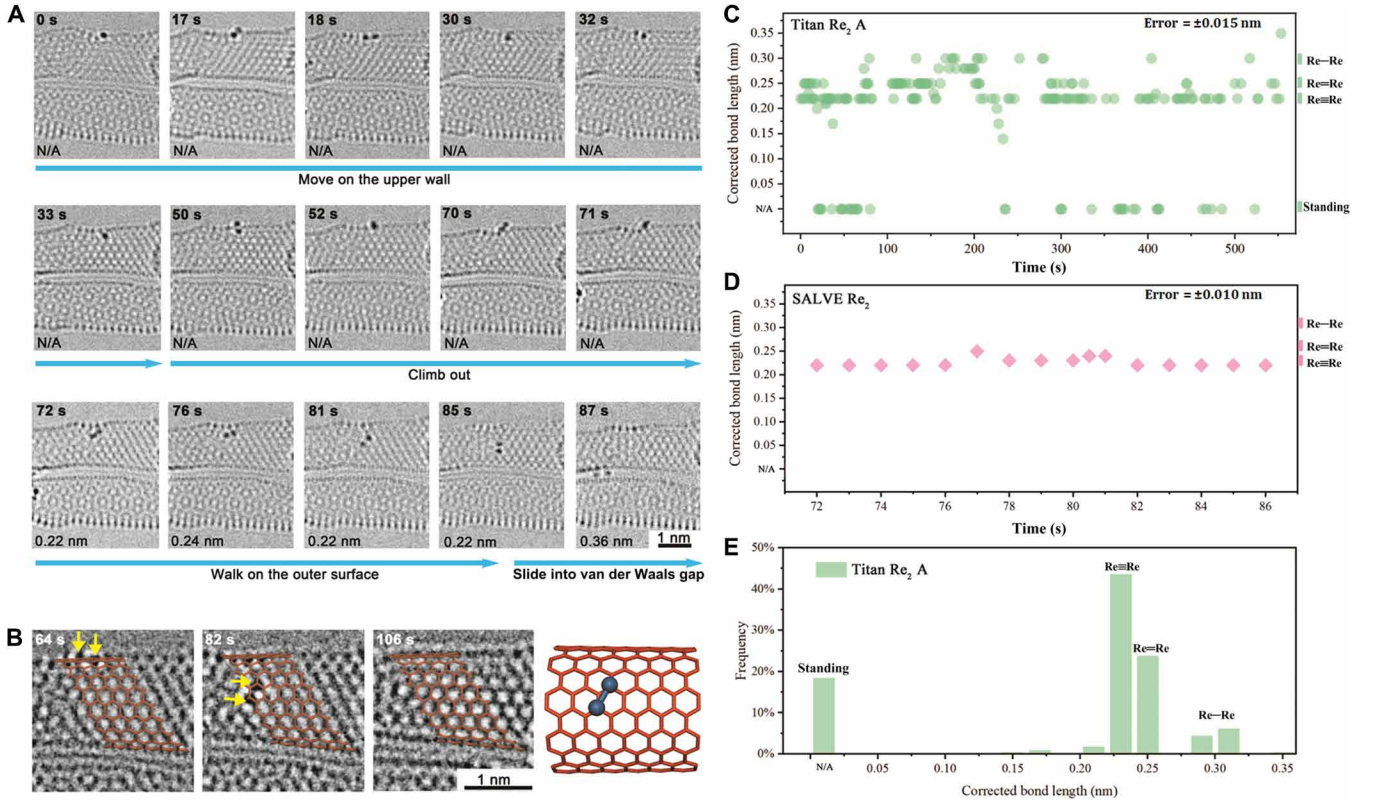

Fig. 2. Changes in Re–Re bond length over time. (**A**) Time-series AC-HRTEM images (80 kV) (unprocessed data) of the first stage of movie S2 acquired by the SALVE TEM. At this stage, the dirhenium molecule moves at a defect site on the SWNT, climbs out from the defect, and then slides into the vdW gap between two parallel SWNTs. The corrected Re–Re bond length of each frame is presented; error is ±0.010 nm. (**B**) Selected frames with adjusted high contrast from movie S2 for analyzing the atomically precise position of the dirhenium molecule when it is drifting along the outer surface of host SWNT. The position of the Re atoms are indicated by yellow arrows. The AC-HRTEM images are partially covered by the model of an SWNT with chirality of (10, 10). The simulated structure shows the position of dirhenium molecule in the frame of 82 s. (**C**) Corrected bond length changing of the right dirhenium molecule in movie S1 (Titan Re_2 A); error is ±0.015 nm. (**D**) Corrected bond length of the dirhenium molecule drifting along the outer wall of SWNT in movie S2 (SALVE Re_2); error is ±0.010 nm. (**E**) The histogram shows the count frequencies of the different bond lengths of Titan Re_2 A (0 to 553 s).

(*24*). From 72 to 85 s, the dirhenium molecule drifts along the outer surface of the host SWNT and then slides into the one-dimensional vdW gap, as indicated by yellow arrows (Fig. 2B). The simulated structure in the right of Fig. 2B shows an atomic structure of the lying orientation of dirhenium molecule in the AC-HRTEM image of 82 s with a Re–Re bond length of 0.22 nm. Figure 2D only shows the bond length changing of the dirhenium molecule when it is drifting along the outer wall before it slides into the vdW gap (72 to 85 s), because the real bond length of Re_2 moving and rotating at the defect site is immeasurable. According to the analysis of the bond length distribution measured over time for the dirhenium molecules (Fig. 2, C to E), the lying orientation with corrected Re–Re bond length of 0.22 nm and the standing orientation with immeasurable bond length are the most common bond structures observed in these two time series, although bond lengths of 0.25 and 0.30 nm are also observed. The measured metallic bond length changes in discrete steps, indicating the existence of single and double Re–Re bonds (Fig. 2C).

The vdW gap between the two parallel SWNTs in the initial state of the second stage (89 s in Fig. 3A) is approximately 0.32 nm (± 0.010 nm), consistent with the theoretical prediction by Lennard-Jones model (*25*). This vdW gap confines Re_2 and provides a one-dimensional channel in the vacuum, limiting Re_2 translation and rotation. In the first 7 s (87 to 94 s) after the dirhenium molecule moves into the vdW gap, the contrast of the Re atoms shows unusual symmetrically elongated features, indicating that the Re atoms are delocalized on the time frame of a single exposure (0.5 s), which may be caused by oscillations along the Re–Re bond, described as a stretch vibration (Fig. 3B). The center distance of the elongated spots is 0.36 nm, which is slightly longer than the Re–Re single bond (around 0.30 nm) in compounds (*21*), while the amplitude of the oscillation of Re atoms is ±0.04 nm. After oscillating for 7 s, Re_2 breaks into two unbound Re atoms with a distance of 0.58 nm (94 s in Fig. 3A and the second column in Fig. 3B). After the separation, the contrast of two Re atoms is no longer elongated and becomes near round. This observation indicates that once the Re–Re bond length exceeds that of a single bond, the molecule may exist in an excited state manifested in a large amplitude of vibrations, and that beyond this critical point, the bond breaks and the two metal atoms separate. In our experiments, Re_2 trapped in the one-dimensional vdW gap acts like a harmonic oscillator, pumped with the kinetic energy transferred from the 80-keV electrons to the Re atom, until it is large enough to overcome the barrier of Re–Re bond dissociation (at 94 s in Fig. 3A). The two Re atoms move freely in the one-dimensional

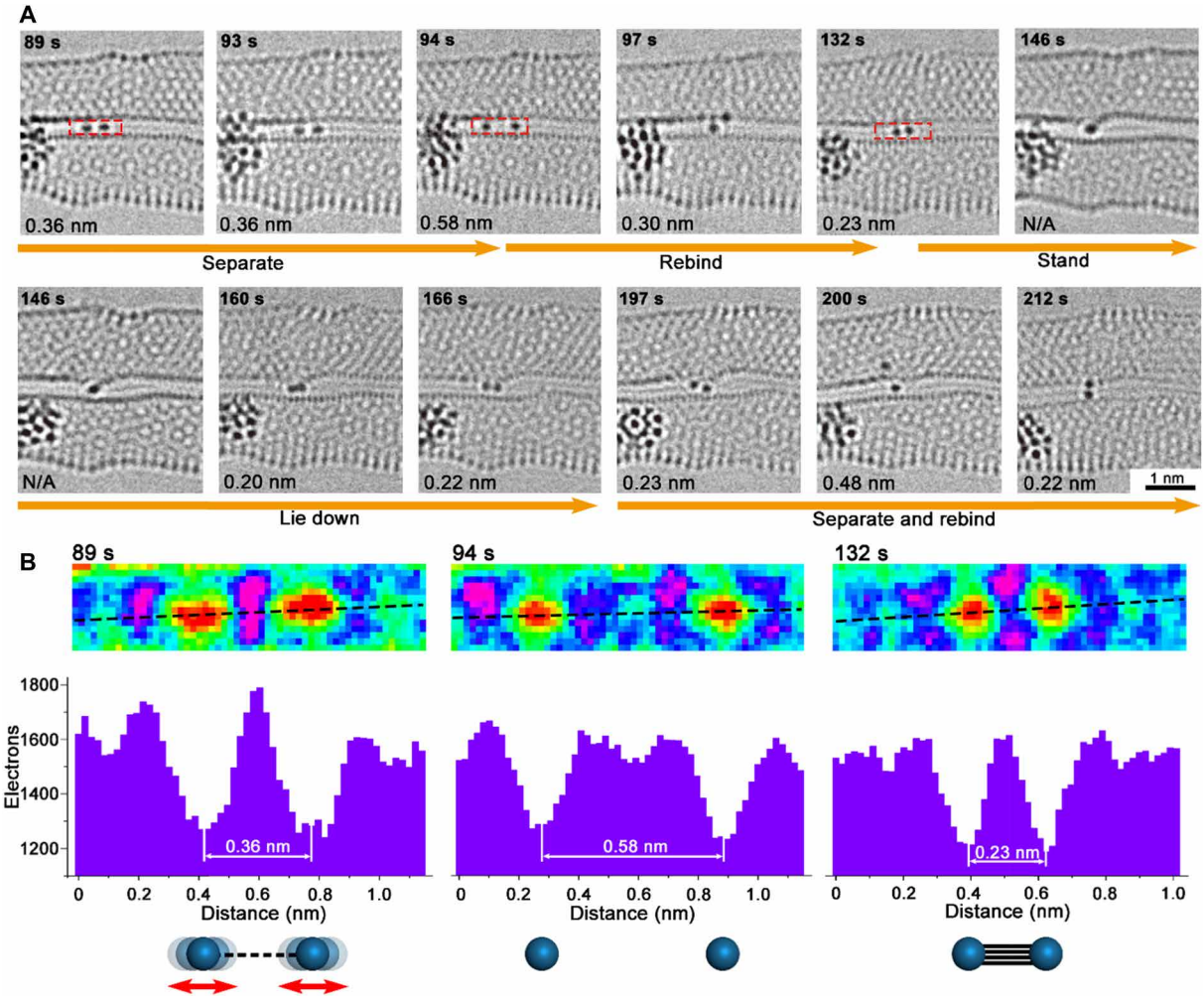

Fig. 3. Atomic-scale dynamics of Re–Re bond dissociation. (**A**) Time-series AC-HRTEM images (80 kV) (unprocessed data) of the second stage of movie S2 acquired by the SALVE TEM. At this stage, the dirhenium molecule confined in the vdW gap shows various dynamic processes. The metallic bonds between two Re atoms break and rebind twice. The dirhenium molecule also stands and lies down in the gap. (**B**) In the first row, false-color images of the red dashed line framed areas in the AC-HRTEM images of 89, 94, and 132 s in (A). The second row shows the intensity profiles of the corresponding black dashed line in the false-color images of the same column. The distances between two Re atoms are measured with an error of ±0.010 nm. The third row shows the possible state of the two Re atoms in each image of the first row.

vdW gap until they collide and recombine into Re_2 at 97 s. The bond distance of the reformed Re_2 reduces from 0.30 (97 s) to 0.23 nm (132 s). The contrast of two Re atoms in the frame of 132 s are near round with a distance of 0.23 nm, indicating that the two Re atoms are bound again by a quadruple bond. This reformed dirhenium molecule shows the same properties as before, moving between different orientations in the one-dimensional vdW gap in the following 34 s, similar to the behavior inside and on the SWNT. In addition, the free Re atom is chemically active toward SWNT, as shown in our previous work (*26*), and interacts with the upper SWNT restructuring the carbon lattice at 97 s. At 200 s, Re_2 dissociates again and recombines at 212 s. This dirhenium molecule moves in the vdW gap in the following 181 s and merges into the large Re cluster in the lower SWNT as shown in movie S2.

DFT calculations have been carried out to elucidate the stable configurations and electronic structure of Re_2 bonded to SWNT (Fig. 4). As discussed in Materials and Methods, a search of possible stable bonding configurations inside the SWNT revealed only the presence of a single standing mode with a Re–Re bond length of 0.22 nm, in which Re_2 bonds in an η^6-mode to all six carbon atoms of a single hexagon with a "4 + 2" asymmetry introduced by the curvature of the nanotube wall. The binding energy of this configuration is −165 kJ/mol (−1.71 eV), relative to the separated dirhenium molecule and SWNT. On the outside of the nanotube, the η^6-standing configuration is again found to be the lowest energy orientation, but the change in curvature introduces several stable lying configurations, which are local minima at higher energy, geometrically and energetically similar to one another (fig. S7).

To understand the bonding configurations observed, it is instructive to examine the spatial extent of the molecular orbitals involved in the bonding. The atomic Re orbitals and the occupied and low-lying unoccupied orbitals of Re_2 are presented in fig. S4, and the electronic structure of the dirhenium molecule is discussed in more detail in the Supplementary Materials. The highest occupied molecular orbital (HOMO) [singly occupied molecular orbital (SOMO)] of the bound species in the standing configuration corresponds to the HOMO

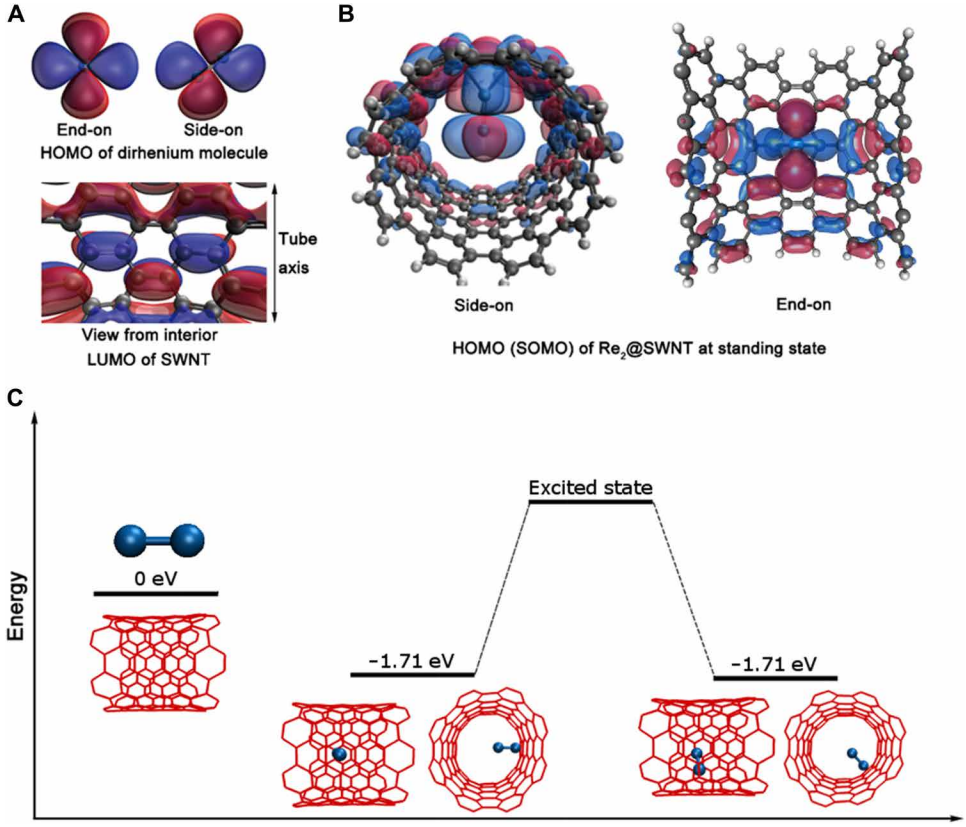

Fig. 4. Interactions of Re_2 with carbon nanotube. (**A**) Comparison of the spatial extent of the Re_2 HOMO (SOMO) viewed end-on and side-on; the overlap with electron density of the SWNT LUMO sufficient for bonding is only achieved when Re_2 approaches the nanotube wall in the end-on orientation. (**B**) Side-on and end-on views of the HOMO (SOMO) of the bound configuration, showing the contraction of the (blue) orbital lobes that maximizes bonding overlap (in the end-on view, some carbon atoms have been removed and the electron density isovalue has been increased to aid visualization). (**C**) Illustration of the dynamics of the dirhenium molecule in the SWNT, with the associated calculated energies relative to the separated molecule and SWNT (left), and front and side views of each state.

(SOMO) of the isolated Re_2, but with contraction of the orbital lobes that are perpendicular to the nanotube axis (Fig. 4B). This maximizes the overlap with the two carbon atoms that are closer to the dirhenium due to the curvature-induced 4 + 2 asymmetry (shown in blue in Fig. 4A). The "end-on" standing η^6-bonding is more stable than "side-on" lying bonding, as this provides a better orbital overlap between the Re_2 HOMO and the SWNT LUMO, in terms of size, shape, and ease of the above orbital contraction. On the outside of the SWNT, the rhenium dimer encounters the convex curvature of the nanotube, and two carbon atoms lie further from the dimer than the other four. The orbital contraction is therefore less pronounced, and the larger orbital lobes presented by the side-on orientation of dirhenium are able to take part in stable bonding with the nanotube wall. Note that the curvature of the SWNT wall is, in turn, affected by the dirhenium molecule, exhibiting a slight flattening of the wall in the region of the bonding, as can be seen in the side views in Fig. 4C. Our calculations predict the presence of standing configurations inside the nanotube; the presence of stable lying configurations could be caused by the different curvature of SWNTs with different diameters. As the bonding modes available to Re_2 seem to be largely influenced by the curvature of the SWNT wall, it is reasonable to assume that the wider nanotube with a smaller degree of curvature imposes less of a restriction on the possible bonding modes and behaves more similarly to the outside of the tube. In addition, the presence of defects and deformations in the SWNT under electron irradiation were not considered in our simulations but may affect the bonding between dirhenium and the SWNT.

Using our experimental observations in conjunction with the theoretical modeling, Fig. 4C illustrates a plausible energy profile for the movement of Re_2 along the nanotube. We propose that, upon elimination of the CO ligands from the precursor molecule, Re_2 bonds to the interior of the SWNT wall, a process we predict to be strongly thermodynamically (−165 kJ/mol binding energy) and kinetically (no energy barrier) favorable. On the order of seconds in our conditions, the electron beam transfers energy to excite Re_2, from which the molecule can relax into adjacent energy minima (Fig. 4C). The absence of any local minima in which Re_2 exists inside the SWNT without being bonded to the walls explains the observed stepwise motion of the dirhenium molecule under electron irradiation, as these would result in a more long-range migration process.

We show that the simultaneous function of the electron beam as a source of energy and an imaging tool allows advancement in the understanding of metallic bonding. The rhenium homonuclear diatomic molecules Re_2 are created in nanotubes in situ under AC-HRTEM observation, and dynamics of Re_2 are imaged with atomic resolution. The metallic bond can change over time as a result of the electron beam effect, most frequently adopting a quadruple bond order. Re_2 can reversibly dissociate to independent atoms under

the electron beam, which transfers up to ~1 eV (~100 kJ/mol) to a Re atom, directly observed when the molecule is confined in the one-dimensional gap between two parallel NTs. An unexpected bonding state where the Re-Re bond order is less than one, accompanied with a large amplitude of vibration observed just before the bond dissociation, indicates the existence of previously unknown bonding states between metal atoms. A combination of DFT calculations and AC-HRTEM time-resolved experiments sheds light on the atomistic mechanism of metallic bond dynamics in real time and direct space, opening up avenues for discovery of new inorganic and organometallic species by electron microscopy methods, such as predicted W_2 with quintuple bond or Re_3 clusters, and exploration of their physical properties and chemical reactivity at the level of the single atom.

MATERIALS AND METHODS

Synthesis of dirhenium molecules confined in SWNTs

SWNTs (Carbon Solutions, USA) were thermally treated to open the ends of the nanotubes and to remove the residual amorphous carbon from the outer walls of the SWNTs before use. The as-received SWNTs were heated in air for 30 min at 600°C with a weight loss of approximately 30% observed for samples. The freshly opened SWNTs were mixed with a twofold by weight excess of $Re_2(CO)_{10}$ compound (Sigma-Aldrich). The resultant mixture was then sealed in a Pyrex glass tube under reduced pressure (10^{-6} mbar) and heated to 150°C for 3 days. The sample was then rapidly cooled to room temperature, and the SWNTs were washed with tetrahydrofuran (100 ml) to remove any species from the outside of the nanotube and filtered through a polytetrafluoroethylene membrane (pore size = 0.2 μm). The sample was then dispersed in isopropanol and drop cast onto a lacey carbon-coated copper TEM grid for HRTEM analysis. The formation of dirhenium molecules can also be achieved by heating $Re_2(CO)_{10}$@SWNT at high temperature. This was achieved by sealing $Re_2(CO)_{10}$@SWNT under argon in a Pyrex tube and heating at 500°C for 3 hours. Rhenium cluster@SWNT samples prepared in this way were identical to the samples formed via electron beam–induced elimination of CO ligands from $Re_2(CO)_{10}$. FTIR measurement shown in fig. S1 confirms the removal of CO from nanotubes during the heating process.

Electron microscopy

AC-HRTEM images in movie S1 were carried out using an image side C_S-corrected FEI Titan 80-300 TEM operated at 80 kV accelerating voltage with a modified filament extraction voltage for information limit enhancement. Images were recorded on a slow-scan charge-coupled device camera type Gatan UltraScan 1000XP. Because a certain amount of electron dose was required to achieve atomic resolution, the exposure time for each frame was 1.0 s. The dose rate of e-beam applied in movie S1 was 1.05×10^8 e^- nm^{-2} s^{-1}.

AC-HRTEM images in movie S2 were carried out using the image side C_C/C_S-corrected SALVE instrument (20 to 80 kV) operated at 80 kV accelerating voltage with a point resolution of <0.08 nm. The exposure time for the frames in movie S2 was 0.5 s. The dose rate of e-beam applied in movie S1 was 1.05×10^8 e^- nm^{-2} s^{-1}. The dose rate of e-beam applied in movie S2 was 1.10×10^8 e^- nm^{-2} s^{-1}.

For each observation, approximately 30 s were spent for adjusting the magnification, dose rate, and focal length. All imaging experiments were carried out at room temperature. In addition, 26 s (from 252 to 278 s) was spent for centering the drifted SWNT in movie S1 during continuous irradiation.

Computational methods

DFT simulations were performed to find stable bonding configurations of the dirhenium molecule with the host SWNT. Rhenium atoms were modeled with the BLYP/SRSC functional/effective core potential pairing, with carbon and hydrogen atoms modeled with a BLYP/6-31G* functional/basis set pairing for initial geometry optimizations, followed by optimizations using BLYP/6-311G* (see the Supplementary Materials for more information on the choice of DFT method). Grimme's empirical DFT-D3(BJ) model (*27*) was used to account for the effects of dispersion. The reported binding energy was corrected for basis set superposition error by using the counterpoise method. The hydrogenated (8,8) SWNT shown in fig. S6 was used as a model nanotube, with a diameter of 1.1 nm compared to the experimental (16,1) SWNT with a diameter of 1.3 nm. The optimized rhenium dimer was placed in initial positions corresponding to those in fig. S5 as well as several different nonbonded positions in the center of the SWNT, and all atom positions (including Re_2) were fully optimized. On the inside of the SWNT, all optimizations resulted in the formation of a standing bonding configuration centered over a hexagon in the tube (shown in Fig. 4). On the outside of the tube, the equivalent hexagon-centered standing bonding configuration was the lowest energy structure, but there were also several additional bonding configurations (shown in fig. S7). The Mulliken charge distribution of the bonded standing state found in the DFT calculations is shown in fig. S8.

SUPPLEMENTARY MATERIALS

Supplementary material for this article is available at http://advances.sciencemag.org/cgi/content/full/6/3/eaay5849/DC1

Section S1. Re_2 electronic structure and choice of functional

Fig. S1. Infrared spectra of Re_2 precursor before and after removal of CO ligands.

Fig. S2. Analysis of a typical migration process repeatedly observed in our TEM experiment.

Fig. S3. Schematic diagram explaining the method for calculating the real bond length between two Re atoms in Re_2 by correcting the measured projected bond length.

Fig. S4. Shapes and energies of Re_2 orbitals.

Fig. S5. Possible configurations of Re_2 lying on the graphitic structure.

Fig. S6. The model SWNT system used in the DFT calculations discussed in the text.

Fig. S7. Configurations of Re_2 outside SWNT with respect to the nanotube lattice.

Fig. S8. The Mulliken charge distribution of the bonded standing state found in the DFT calculations.

Movie S1. Dynamics of two Re_2 molecules confined in SWNT stimulated and imaged by electron beam in Titan TEM at 80 kV.

Movie S2. Dynamics of one Re_2 molecule stimulated and imaged by electron beam in SALVE TEM at 80 kV.

References (*28*–*39*)

REFERENCES AND NOTES

1. F. A. Cotton, Carlos A. Murillo, Richard A. Walton, *Multiple Bonds Between Metal Atoms* (Springer Science and Business Media, 2005).
2. F. A. Cotton, N. F. Curtis, C. B. Harris, B. F. G. Johnson, S. J. Lippard, J. T. Mague, W. R. Robinson, J. S. Wood, Mononuclear and polynuclear chemistry of rhenium (III): Its pronounced homophilicity. *Science* **145**, 1305–1307 (1964).
3. F. A. Cotton, Metal-metal bonding in $[Re_2X_8]^{2-}$ ions and other metal atom clusters. *Inorg. Chem.* **4**, 334–336 (1964).
4. T. Nguyen, A. D. Sutton, M. Brynda, J. C. Fettinger, G. J. Long, P. P. Power, Synthesis of a stable compound with fivefold bonding between two chromium(I) centers. *Science* **310**, 844–847 (2005).
5. F. R. Wagner, A. Noor, R. Kempe, Ultrashort metal–metal distances and extreme bond orders. *Nat. Chem.* **1**, 529–536 (2009).
6. K. A. Kreisel, G. P. A. Yap, O. Dmitrenko, C. R. Landis, K. H. Theopold, The shortest metal-metal bond yet: Molecular and electronic structure of a dinuclear chromium diazadiene complex. *J. Am. Chem. Soc.* **129**, 14162–14163 (2007).

7. A. Noor, G. Glatz, R. Mueller, M. Kaupp, S. Demeshko, R. Kempe, Carboalumination of a chromium–chromium quintuple bond. *Nat. Chem.* **1**, 322–325 (2009).
8. G. Merino, K. J. Donald, J. S. D'Acchioli, R. Hoffmann, The many ways to have a quintuple bond. *J. Am. Chem. Soc.* **129**, 15295–15302 (2007).
9. B. O. Roos, P.-Å. Malmqvist, L. Gagliardi, Exploring the actinide-actinide bond: Theoretical studies of the chemical bond in Ac_2, Th_2, Pa_2, and U_2. *J. Am. Chem. Soc.* **128**, 17000–17006 (2006).
10. L. Gagliardi, B. O. Roos, Quantum chemical calculations show that the uranium molecule U_2 has a quintuple bond. *Nature* **433**, 848–851 (2005).
11. Z. Hu, B. Shen, Q. Zhou, S. Deosaran, J. R. Lombardi, D. M. Lindsay, W. Harbich, Raman spectra of mass-selected vanadium dimers in argon matrices. *J. Chem. Phys.* **95**, 2206–2209 (1991).
12. Z. Hu, J.-G. Dong, J. R. Lombardi, D. M. Lindsay, W. Harbich, Absorption, fluorescence, and Raman spectra of mass-selected rhenium dimers in argon matrices. *J. Chem. Phys.* **101**, 95–103 (1994).
13. L. R. Liu, J. D. Hood, Y. Yu, J. T. Zhang, N. R. Hutzler, T. Rosenband, K.-K. Ni, Building one molecule from a reservoir of two atoms. *Science* **360**, 900–903 (2018).
14. M. Linck, P. Hartel, S. Uhlemann, F. Kahl, H. Müller, J. Zach, M. Haider, M. Niestadt, M. Bischoff, J. Biskupek, Z. Lee, T. Lehnert, F. Börrnert, H. Rose, U. Kaiser, Chromatic aberration correction for atomic resolution TEM imaging from 20 to 80 kV. *Phys. Rev. Lett.* **117**, 076101 (2016).
15. S. T. Skowron, T. W. Chamberlain, J. Biskupek, U. Kaiser, E. Besley, A. N. Khlobystov, Chemical reactions of molecules promoted and simultaneously imaged by the electron beam in transmission electron microscopy. *Acc. Chem. Res.* **50**, 1797–1807 (2017).
16. K. Cao, T. W. Chamberlain, J. Biskupek, T. Zoberbier, U. Kaiser, A. N. Khlobystov, Direct correlation of carbon nanotube nucleation and growth with the atomic structure of rhenium nanocatalysts stimulated and imaged by the electron beam. *Nano Lett.* **18**, 6334–6339 (2018).
17. K. Cao, T. Zoberbier, J. Biskupek, A. Botos, R. L. McSweeney, A. Kurtoglu, C. T. Stoppiello, A. V. Markevich, E. Besley, T. W. Chamberlain, U. Kaiser, A. N. Khlobystov, Comparison of atomic scale dynamics for the middle and late transition metal nanocatalysts. *Nat. Commun.* **9**, 3382 (2018).
18. A. W. Robertson, B. Montanari, K. He, J. Kim, C. S. Allen, Y. A. Wu, J. Olivier, J. Neethling, N. Harrison, A. I. Kirkland, J. H. Warner, Dynamics of single Fe atoms in graphene vacancies. *Nano Lett.* **13**, 1468–1475 (2013).
19. T. Susi, J. Kotakoski, D. Kepaptsoglou, C. Mangler, T. C. Lovejoy, O. L. Krivanek, R. Zan, U. Bangert, P. Ayala, J. C. Meyer, Q. Ramasse, Silicon–carbon bond inversions driven by 60-keV electrons in graphene. *Phys. Rev. Lett.* **113**, 115501 (2014).
20. M. Tripathi, A. Mittelberger, N. A. Pike, C. Mangler, J. C. Meyer, M. J. Verstraete, J. Kotakoski, T. Susi, Electron-beam manipulation of silicon dopants in graphene. *Nano Lett.* **18**, 5319–5323 (2018).
21. O. Cretu, A. V. Krasheninnikov, J. A. Rodríguez-Manzo, L. Sun, R. M. Nieminen, F. Banhart, Migration and localization of metal atoms on strained graphene. *Phys. Rev. Lett.* **105**, 196102 (2010).
22. N. I. Gapotchenko, N. V. Alekseev, N. E. Kolobova, K. N. Anisimov, I. A. Ronova, A. A. Johansson, Molecular structure of dirhenium decacarbonyl. *J. Organomet. Chem.* **35**, 319–320 (1972).
23. S. Hu, M. Lozada-Hidalgo, F. C. Wang, A. Mishchenko, F. Schedin, R. R. Nair, E. W. Hill, D. W. Boukhvalov, M. I. Katsnelson, R. A. W. Dryfe, I. V. Grigorieva, H. A. Wu, A. K. Geim, Proton transport through one-atom-thick crystals. *Nature* **516**, 227–230 (2014).
24. A. N. Andriotis, M. Menon, G. Froudakis, Catalytic action of Ni atoms in the formation of carbon nanotubes: A molecular dynamics study. *Phys. Rev. Lett.* **85**, 3193–3196 (2004).
25. C.-H. Sun, G.-Q. Lu, H.-M. Cheng, Simple approach to estimating the van der Waals interaction between carbon nanotubes. *Phys. Rev. B* **73**, 195414 (2006).
26. T. W. Chamberlain, J. C. Meyer, J. Biskupek, J. Leschner, A. Santana, N. A. Besley, E. Bichoutskaia, U. Kaiser, A. N. Khlobystov, Reactions of the inner surface of carbon nanotubes and nanoprotrusion processes imaged at the atomic scale. *Nat. Chem.* **3**, 732–737 (2011).
27. S. Grimme, S. Ehrlich, L. Goerigk, Effect of the damping function in dispersion corrected density functional theory. *J. Comput. Chem.* **32**, 1456–1465 (2011).
28. A. C. Borin, J. Paulo Gobbo, B. O. Roos, Electronic structure and chemical bonding in the ground states of Tc_2 and Re_2. *Mol. Phys.* **107**, 1035–1040 (2009).
29. C. J. Cramer, D. G. Truhlar, Density functional theory for transition metals and transition metal chemistry. *Phys. Chem. Chem. Phys.* **11**, 10757–10816 (2009).
30. Z. J. Wu, B. Han, Z. W. Dai, P. C. Jin, Electronic properties of rhenium, osmium and iridium dimers by density functional methods. *Chem. Phys. Lett.* **403**, 367–371 (2005).
31. X. Sun, J. Du, P. Zhang, G. Jiang, A systemic DFT study on several 5d-electron element eimers: Hf_2, Ta2, Re_2, W_2, and Hg_2. *J. Clust. Sci.* **21**, 619–636 (2010).
32. R.-N. Zhao, R. Chen, Y.-H. Yuan, J.-G. Han, Y. Duan, Computational investigation on the structures and electronic properties of the nanosized rhenium clusters. *Solid State Ionics* **310**, 24–29 (2017).
33. J. P. Perdew, K. Burke, M. Ernzerhof, Generalized gradient approximation made simple. *Phys. Rev. Lett.* **77**, 3865–3868 (1996).
34. A. D. Becke, Density-functional exchange-energy approximation with correct asymptotic behaviour. *Phys. Rev. A* **38**, 3098–3100 (1988).
35. C. Lee, W. Yang, R. G. Parr, Development of the Colle-Salvetti correlation-energy formula into a functional of the electron density. *Phys. Rev. B* **37**, 785–789 (1988).
36. Y. Zhao, D. G. Truhlar, A new local density functional for main-group thermochemistry, transition metal bonding, thermochemical kinetics, and noncovalent interactions. *J. Chem. Phys.* **125**, 194101 (2006).
37. P. J. Hay, W. R. Wadt, *Ab initio* effective core potentials for molecular calculations. Potentials for K to Au including the outermost core orbitals. *J. Chem. Phys.* **82**, 299–310 (1985).
38. D. Andrae, U. Häußermann, M. Dolg, H. Stoll, H. Preuß, Energy-adjusted *ab initio* pseudopotentials for the second and third row transition elements. *Theor. Chim. Acta* **77**, 123–141 (1990).
39. F. Weigend, R. Ahlrichs, Balanced basis sets of split valence, triple zeta valence and quadruple zeta valence quality for H to Rn: Design and assessment of accuracy. *Phys. Chem. Chem. Phys.* **7**, 3297–3305 (2005).

Acknowledgments

Funding: K.C. acknowledges China Scholarship Council (CSC) for financial support. K.C., J.B., and U.K. acknowledge the support of the "Graphene Flagship" and the DFG and the Ministry of Science, Research and the Arts (MWK) of Baden-Württemberg within the frame of the SALVE (Sub Angstrom Low-Voltage Electron Microscopy) project. A.N.K. acknowledges the Engineering and Physical Sciences Research Council (EPSRC) for financial support and the Nanoscale and Microscale Research Centre (nmRC) and Centre for Sustainable Chemistry (CSC), University of Nottingham, for access to instrumentation. S.T.S. and E.B. are grateful to the High Performance Computing (HPC) Facility at the University of Nottingham for providing computational time. **Author contributions:** C.T.S. prepared the samples of $Re_2(CO)_{10}$ molecules confined in SWNTs and performed FTIR measurements supervised by A.N.K. A.N.K. preinvestigated the sample using uncorrected TEM. K.C. investigated the samples using spherical aberration-corrected TEM, and K.C. and J.B. investigated the samples using chromatic and spherical aberration-corrected TEM (SALVE TEM); U.K. supervised the TEM work. K.C. discovered the dirhenium molecules. S.T.S. carried out the DFT calculations supervised by E.B. C. L. contributed to data analysis. All authors discussed the results and interpreted the data. K.C. drafted the initial manuscript, and A.N.K. and U.K. refined it. All the authors contributed to writing and further refining of the manuscript. **Competing interests:** The authors declare that they have no competing interests. **Data and materials availability:** All data needed to evaluate the conclusions in the paper are present in the paper and/or the Supplementary Materials. Additional data related to this paper may be requested from the authors.

Submitted 1 July 2019
Accepted 19 November 2019
Published 17 January 2020
10.1126/sciadv.aay5849

Citation: K. Cao, S. T. Skowron, J. Biskupek, C. T. Stoppiello, C. Leist, E. Besley, A. N. Khlobystov, U. Kaiser, Imaging an unsupported metal–metal bond in dirhenium molecules at the atomic scale. *Sci. Adv.* **6**, eaay5849 (2020).

Science Advances

Imaging an unsupported metal–metal bond in dirhenium molecules at the atomic scale

Kecheng Cao, Stephen T. Skowron, Johannes Biskupek, Craig T. Stoppiello, Christopher Leist, Elena Besley, Andrei N. Khlobystov and Ute Kaiser

Sci Adv **6** (3), eaay5849.
DOI: 10.1126/sciadv.aay5849